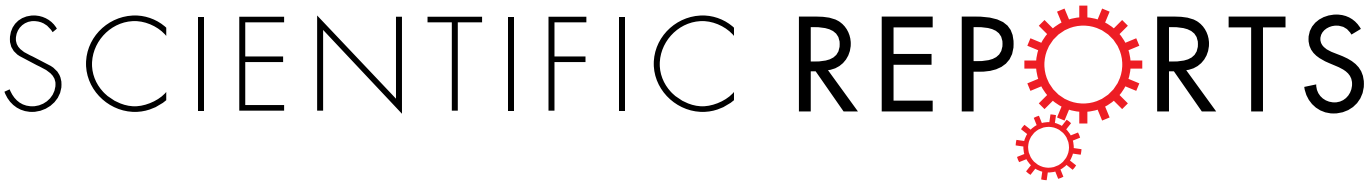

OPEN

Decadal trends in Red Sea maximum surface temperature

V. Chaidez[1], D. Dreano[2], S. Agusti[1], C. M. Duarte[1] & I. Hoteit[3]

Received: 1 February 2017
Accepted: 5 July 2017
Published online: 15 August 2017

Ocean warming is a major consequence of climate change, with the surface of the ocean having warmed by 0.11 °C decade^{-1} over the last 50 years and is estimated to continue to warm by an additional 0.6–2.0 °C before the end of the century[1]. However, there is considerable variability in the rates experienced by different ocean regions, so understanding regional trends is important to inform on possible stresses for marine organisms, particularly in warm seas where organisms may be already operating in the high end of their thermal tolerance. Although the Red Sea is one of the warmest ecosystems on earth, its historical warming trends and thermal evolution remain largely understudied. We characterized the Red Sea's thermal regimes at the basin scale, with a focus on the spatial distribution and changes over time of sea surface temperature maxima, using remotely sensed sea surface temperature data from 1982–2015. The overall rate of warming for the Red Sea is 0.17 ± 0.07 °C decade^{-1}, while the northern Red Sea is warming between 0.40 and 0.45 °C decade^{-1}, all exceeding the global rate. Our findings show that the Red Sea is fast warming, which may in the future challenge its organisms and communities.

Ocean warming with climate change[1] is creating challenges for organisms, which accommodate to warming by shifting their distribution poleward and advancing their phenology[2]. While parts of the ocean may be warming gradually, others may experience rapid fluctuations, tipping points, or extreme weather events, such as heat waves, likely inducing greater impacts on biodiversity[1,3], as exemplified by the impacts of heat waves on seagrass[4,5] and other organisms in the Mediterranean, a rapidly warming sea[6]. Extreme heat events such as ocean heat waves propagated by El Niño-Southern Oscillation are also major concerns for coral reefs as they may lead to bleaching[7–9]. The magnitude and duration of such events is important for organisms experiencing temperature anomalies outside their optimal thermal range and perhaps even above their thermal limits. High temperature anomalies of air and water are also linked to stratification of the water column, potentially diminishing oxygen levels and/or increasing microbial virulence, thus causing mass mortality of organisms and disrupting community structure[10–12].

Impacts of warming are likely to be greatest in semi-enclosed seas, which tend to support warming rates faster than average[5,13] and where the capacity of organisms to adapt to warming by shifting their biogeographical range poleward is limited by the presence of continental masses[14], rendering most semi-enclosed seas climatic sink areas for marine organisms[15].

The Red Sea is a semi-enclosed, extremely warm sea basin, experiencing rapid warming[16–19]. Between 1982 and 2006, the average annual temperature of the Red Sea increased by 0.74 °C[17], comparable to the global average of 0.85 °C[1]. An intense warming event occurred in 1994 leading to a 0.7 °C increase in mean annual SST (sea surface temperature)[18]. Modern average temperatures in the Red Sea already exceed those of other tropical regions[20,21]. Although it is considered a fast warming, large marine ecosystem, its thermal regimes and evolution remain largely unresolved[17,22]. Yet, the Red Sea hosts one of the largest reef systems in the world, where organisms may be already close to their thermal limits.

Whereas most analyses focus on mean seawater temperature, maximum temperature may be a more relevant property in relation to some specific questions. For instance, thermal collapse is determined by temperature exceeding the thermal capacity of organisms[23], which is, therefore, dependent on the maximum, rather than the mean temperature the organisms experience. This may be particularly important in the Red Sea where maximum

[1]King Abdullah University of Science and Technology (KAUST), Red Sea Research Center (RSRC), Thuwal, 23955-6900, Saudi Arabia. [2]King Abdullah University of Science and Technology (KAUST), Computer, Electrical and Mathematical Sciences and Engineering Division (CEMSE), Thuwal, 23955-6900, Saudi Arabia. [3]King Abdullah University of Science and Technology (KAUST), Physical Sciences and Engineering Division, Thuwal, 23955-6900, Saudi Arabia. Correspondence and requests for materials should be addressed to V.C. (email: veronica.chaidez@kaust.edu.sa)

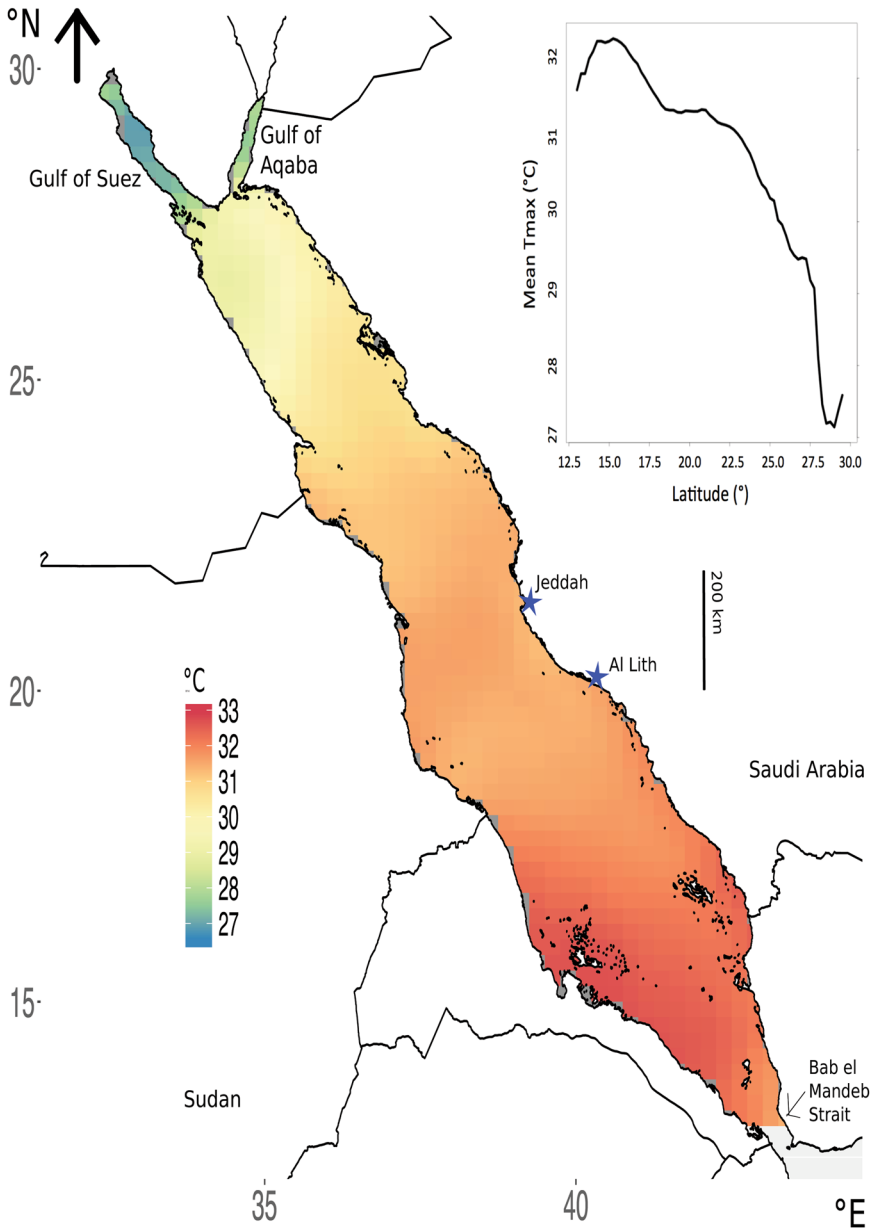

Figure 1. Distribution of mean (from 1982 to 2015) maximum annual temperature (T_{max}) across the Red Sea. Insert shows the latitudinal changes in mean (from 1982 to 2015) T_{max}. Values based on daily temperature data. Image created using R (v3.3.1, www.R-project.org)[45] including packages: ggplot2[46] and rasterVis[47], RStudio (v1.0.143, www.rstudio.com), and InkScape (v0.91, www.inkscape.org).

seawater temperatures are already extremely high. Yet, available analyses of thermal regimes in the Red Sea focus on annual mean values[18,19,24,25], rather than the dynamics of maximum temperature. Here we characterize the variability in temperature maxima across the Red Sea and over time (1982 to 2015), based on daily values, identifying rates of change in annual maximum sea surface temperature, hereafter T_{max}, as well as the distribution of anomalies, relative to T_{max} over time.

Results

Warming rates and timing. The Red Sea displays a latitudinal gradient of increasing T_{max} from north to south with the southern Red Sea exhibiting the highest T_{max} (33 °C) until the southernmost Bab-el-Mandeb Strait (Fig. 1). The Gulf of Suez and the Gulf of Aqaba both exhibit lower temperatures than the open Red Sea (Fig. 1).

The northern Red Sea experiences T_{max} throughout July while T_{max} is reached between late July and mid–August in the southern Red Sea (Fig. 2). The area off of Al Lith, Saudi Arabia, prominently exhibits delayed T_{max} from approximately mid August to early September (red area in Fig. 2).

We assessed the rate of change in the magnitude and timing of T_{max} across the Red Sea. We observed a significant trend toward increased T_{max} across the Red Sea, at an average rate of 0.17 ± 0.07 °C decade^{-1} ($p = 0.02$,

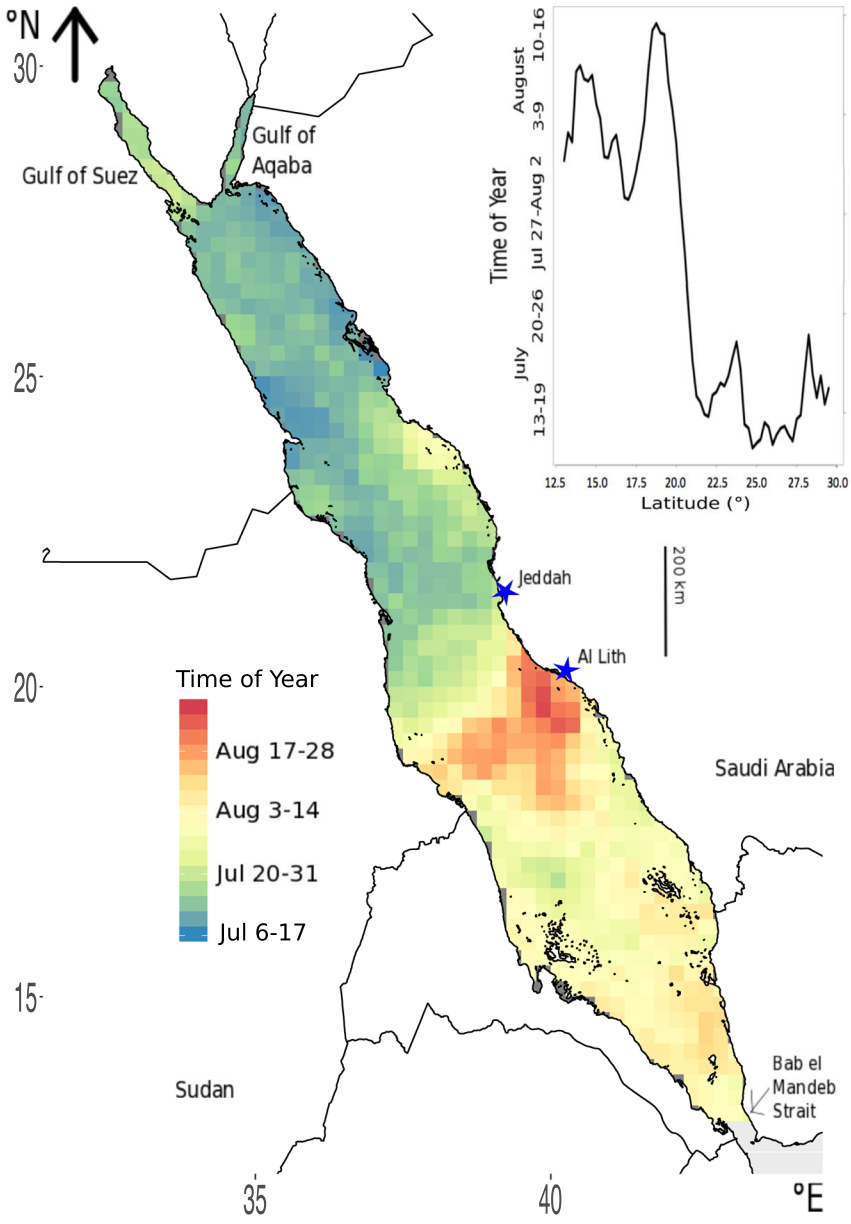

Figure 2. Average yearly timing of maximum annual temperature (T_{max}) across the Red Sea. Insert shows the latitudinal trend in the average timing of T_{max}. Image created using R (v3.3.1, www.R-project.org)[45] including packages: ggplot2[46] and rasterVis[47], RStudio (v1.0.143, www.rstudio.com), and InkScape (v0.91, www.inkscape.org).

df = 32, t = 2.437). Rates of change in T_{max} varied across the Red Sea, with highest rates found in the colder areas of the Red Sea, including the northern Red Sea with rates for the Gulf of Suez and Gulf of Aqaba at 0.40 – 0.45 °C decade^{-1} (Fig. 3a). The region experiencing the lowest rate of warming is, again, that exhibiting a delayed T_{max} off the coast of Al Lith, Saudi Arabia (blue area in Fig. 3a).

In addition to a general pattern toward increasing T_{max}, maximum temperatures in the Red Sea are also being reached earlier, with an average rate of change in the timing of T_{max} of 0.19 ± 0.30 days earlier decade^{-1} (Fig. 3b). Most of the Red Sea experienced progressively earlier T_{max} by 0.1 to 2 days earlier decade^{-1}, but a region in the southern Red Sea showed a delay in T_{max} by 1 to 2 days decade^{-1}. This is the same region that exhibits anomalous trends in the annual timing of T_{max} (Fig. 2).

Heat anomalies. Heat waves representing anomalies of 1.0 °C above the average T_{max} were observed more frequently in the northern half of the Red Sea over the last 34 years. The majority of the basin experienced such anomalies during at least one year and up to 6 years (which may or may not have been successive years). Some areas in the northern Red Sea, including the Gulf of Aqaba, experienced 1.0 °C magnitude heat waves as often as 5 or 6 years over the 34 year period examined here (Fig. 4).

T_{max} values 0.5 °C above the mean (1982 – 2015) values occurred 15 to 24% of the years, whereas thermal anomalies involving T_{max} values 0.75 °C above the mean values occurred 6 to 12% of the years, and years with

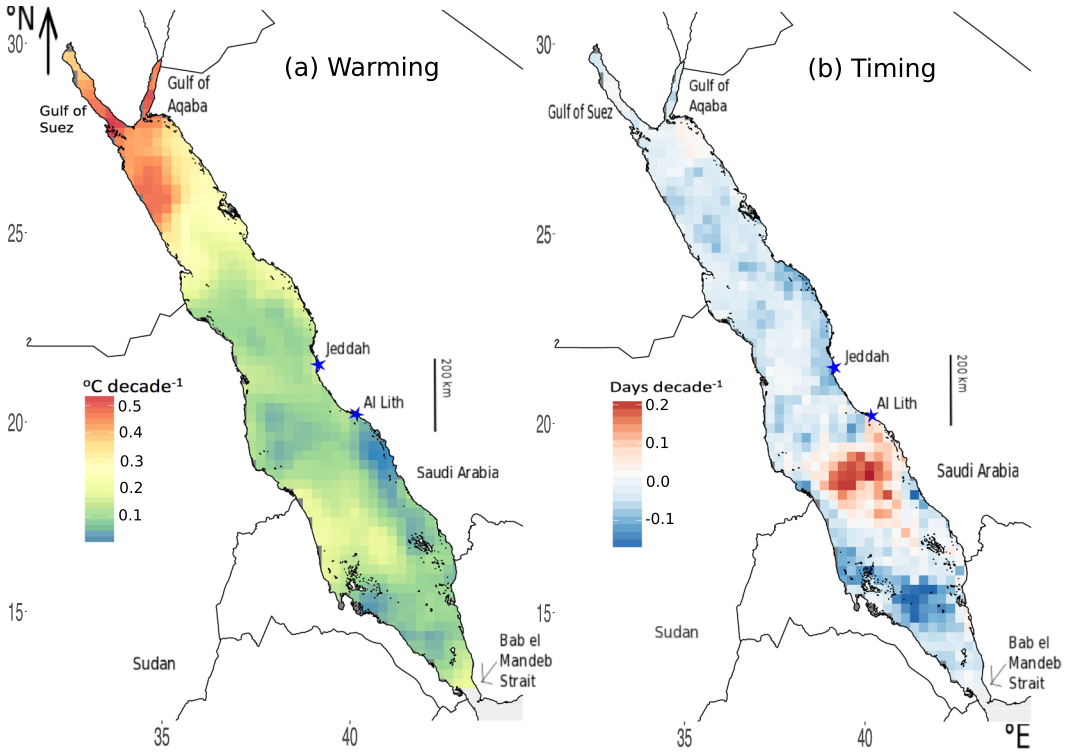

Figure 3. (**a**) Decadal rates of warming (°C decade^{-1}) and (**b**) change in timing (days decade^{-1}) of mean maximum annual temperature (T_{max}) across the Red Sea. Image created using R (v3.3.1, www.R-project.org)[45] including packages: ggplot2[46] and rasterVis[47], RStudio (v1.0.143, www.rstudio.com), and InkScape (v0.91, www.inkscape.org).

T_{max} values of 1.0 °C above the mean values occurred with a probability <6% (Fig. 5). The decline in the frequency of T_{max} anomalies with increasing magnitude of anomalies was significant (Kruskal-Wallis, $p < 2.2\,e^{-16}$, chi-squared = 2674, df = 4, Fig. 5) and significant differences were found among all groups (Dunn's, $p < 0.05$, Z range = [4:44]).

Discussion

The latitudinal gradient of increasing T_{max} from north to south in the Red Sea is largely a consequence of the variation in solar radiation associated with these latitudinal differences, and is consistent with previous studies reporting the same trend based on mean temperatures, with the warmest thermal regime in the southern region[19]. The Gulf of Suez and the Gulf of Aqaba have colder thermal regimes. Previous studies reported that, in the summer, the surface water entering the Gulf of Aqaba from the Red Sea is about 2 °C warmer than the water inside the Gulf[26].

The Red Sea basin presents a discontinuity in terms of the timing of T_{max}, associated with an abrupt transition between 20 and 22 °N. The timing of T_{max} occurs two months earlier south of this boundary compared to the timing north of this boundary. The distinct break between North and South (Fig. 2), may be evidence for the strong coupling of wind and sea surface temperatures over the basin as in other ocean systems[27–29]. During winter (October–April), the basin experiences opposing southward and northward winds, converging at about the same belt between 19 – 20 °N[19] where the divide in timing of T_{max} is observed. From May to September, the major wind vector is from north to south[19].

The warming rate of the Red Sea, 0.17 ± 0.07 °C decade^{-1}, is higher than the global ocean rate of 0.11 °C decade^{-1} [1]. The northern Red Sea is warming faster with the Gulf of Suez and Gulf of Aqaba (0.40 – 0.45 °C decade^{-1}) (Fig. 3a) warming four times faster than the mean global ocean warming rate. The semi-enclosed nature of the two gulfs as well as that of the Red Sea as a whole may account for the intense warming[17,30,31], while the slower rate of increase in the southern Red Sea may be buffered by its closer connection to the Indian Ocean. Although the northern Red Sea is warming faster, it remains the coolest region in the basin throughout the year.

Increased T_{max} will have effects on marine biota, which are particularly vulnerable to heat waves, when their thermal limits may be approached or exceeded[23,32]. The occurrence of heat anomalies, which are also likely to increase in the future[1], are greatly relevant to the physiology of organisms, particularly for those inhabiting already warm environments, like the Red Sea, where temperature anomalies may lead to thermal collapse[24,32–34]. The years 1999 and 2001 experienced the largest anomalies across the basin (Fig. 6). During the years 1997 – 1998, one of the strongest El Niño events occurred, while 2000 – 2001 was considered a weak La Niña event[35]. The years 2003 and 2015, also El Niño years, showed the second greatest percentage of area covered by T_{max} anomalies, although of a relatively small, 0.5 °C, magnitude (Fig. 6).

Systematic monitoring efforts are required to detect the effect of heat anomalies on marine organisms, such as bleaching and mass mortality events[36]. Unfortunately, there is no systematic monitoring of biological events in

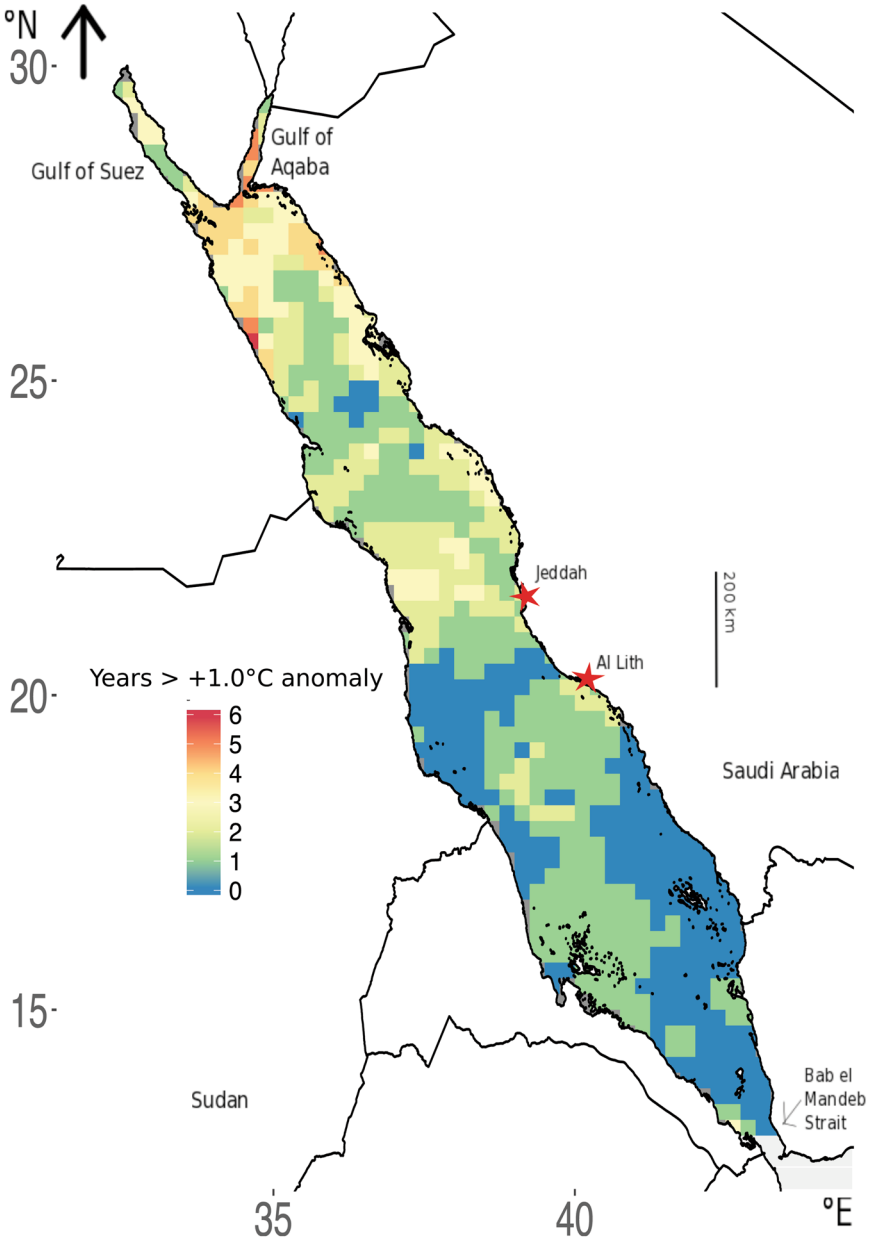

Figure 4. Distribution of the frequency, as number of years, across the Red Sea when maximum annual temperature (T_{max}) reached 1.0 °C higher than the mean T_{max} for 1982–2015. Image created using R (v3.3.1, www.R-project.org)[45] including packages: ggplot2[46] and rasterVis[47], RStudio (v1.0.143, www.rstudio.com), and InkScape (v0.91, www.inkscape.org).

the Red Sea, such as bleaching events, which may be affected by thermal anomalies such as those reported here. Extensive bleaching was reported in the southern half of the Red Sea in 2015, one of the years with extensive, but relatively moderate, thermal anomalies in our analysis (Fig. 6). Whether bleaching events also occurred in other years with extensive T_{max} anomalies is unknown due to lack of long-term monitoring.

The distribution of T_{max} in the Red Sea conforms to the four provinces, described by Raitsos *et al.*[19] based on phytoplankton biomass. The warmer T_{max} regime in the South is associated with higher phytoplankton biomass, while the lowest T_{max} in the northern Red Sea is associated with the lowest phytoplankton biomass. However, this pattern may be a result of the decrease in nutrient concentrations from south to north along the Red Sea[37], rather than its thermal regime. A region in the central Red Sea emerges as deviating from the general pattern with a slower rate of warming and T_{max} reached later in the year over time.

That T_{max} is rapidly increasing in the Red Sea, which is already one of the warmest seas, anticipates challenges to biota. Whereas T_{max} is increasing more rapidly in the North than in the South, the warmer thermal regime in the South may already be near the thermal limits of organisms and, therefore, even a modest increase in T_{max} may suffice to exceed their thermal tolerance, although experimental work is necessary to test this suggestion. Unfortunately, although the Red Sea ranks as the warmest sea on the planet, aside from one study examining the

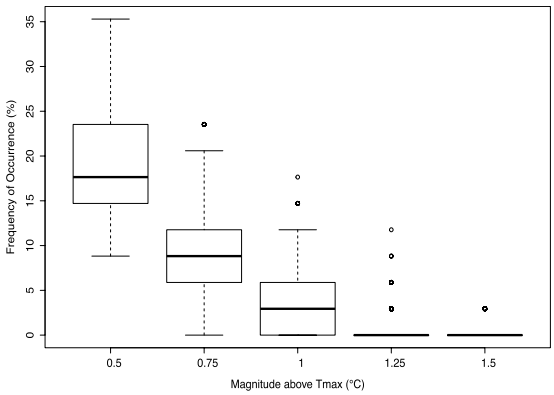

Figure 5. Probability, as the frequency of occurrence between 1982–2015, of maximum annual temperature (T_{max}) anomalies of different magnitudes. A Kruskal-Wallis test and post-hoc Dunn's tests found significantly different frequencies among and between all anomalies (Kruskal-Wallis, $p < 2.2\,e^{-16}$, chi-squared = 2674, df = 4; all Dunn's tests, $p < 0.05$, Z range = [4:44]).

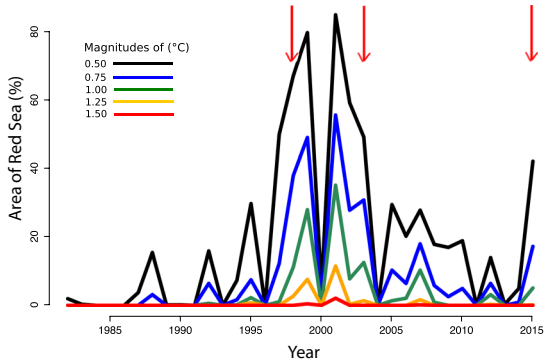

Figure 6. Percent of Red Sea area exhibiting maximum annual temperature (T_{max}) anomalies of different magnitudes between 1982 and 2015. Red indicators signal the occurrence of El Niño events.

effect of temperature on grazing rates of Red Sea parrotfish[38], there is, at present, no quantitative information on the thermal limits of Red Sea biota. However, reports of a decline in coral growth and calcification across the thermal range of Red Sea corals[39], together with widespread bleaching in the southern half of the Red Sea during 2015, as well as lower growth rates reported for brown macroalgae[40], suggests that warm Red Sea temperatures already challenge the capacities of organisms. In addition to increasing T_{max}, the general tendency towards an earlier occurrence indicates that phenology patterns of organisms might need to adjust to this shift. Marine organisms generally cope with warming by shifting their biogeographical range poleward tracking the migration of isotherms[2,14]. However, this strategy is not possible in semi-enclosed seas, such as the Red Sea[14,15], rendering its large pool of endemic species at risk of extinction unless they become Lessepsian migrants and colonize the Mediterranean Sea as a hundred Red Sea species have done[41]. Altogether, higher and earlier T_{max} may challenge the capacities of Red Sea biota to cope.

Results presented here provide a context for experimental analyses examining thermal limits, by defining the regimes and trends in T_{max} across the Red Sea, as well as the likelihood of observing anomalies of different magnitudes. In addition, these results may help understand biodiversity patterns and losses across natural gradients in the Red Sea by matching the distribution of communities and habitats with the distribution of T_{max}. This will provide an underpinning to the assessment thermal maxima play in explaining patterns of biodiversity across the Red Sea.

In conclusion, Red Sea biota are exposed to increased ocean warming, particularly in the northern Red Sea, which may affect their future persistence, especially if unable to migrate into the Mediterranean. The results on Red Sea warming presented here, coupled with experimental evidence on the thermal limits of Red Sea organisms, yet to be resolved, would provide a powerful tool to predict the future of marine biodiversity in this biodiversity hotspot containing a high degree of endemism.

Methods

The dataset. We used remotely sensed sea surface temperature (SST, °C) data to examine maximum temperatures on a basin-wide scale across the Red Sea. The AVHRR–OI (Advanced Very High Resolution Radiometer–Optimum Interpolation) Pathfinder sensor currently provides the longest continuous daily dataset of infrared SST from 1981 to present[42], allowing the assessment of decadal trends of temperatures. Whereas other sensors provide higher resolution, in terms of pixel size, they encompass a period too short to be climatically-relevant as yet (ERS-1/ATSR-1 and Acqua/AMSR-E)[43] and do not allow us to identify, with confidence, the maximum

temperature achieved over time. A daily Level-4, gap-free dataset merging day and night analysis AVHRR SST was obtained from NASA's (National Aeronautics and Space Administration) National Climatic Data Center[44] at podaac.jpl.nasa.gov accessed on January 5, 2016 encompassing 34 years over the period 1982 to 2015. This dataset has been optimally interpolated and mapped on a 0.25° × 0.25° grid. The values in the dataset were corrected with *in situ* measurements from buoys and ships[42]. Daily fluctuations in daily SST time series may significantly affect the measurement of maximum SST phenology and magnitude, because the recurrence of the passage of AVHRR Pathfinder is 2 to 3 days and, the time of passage may not match the time of T_{max}, typically found in the late afternoon with a daily range in T_{max}, derived from moorings in the central Red Sea, of up to 3 °C. Moreover, the individual estimates may be affected by dust, which is prevalent in the region at the time of T_{max}, and cloud cover. Whereas the data we used is interpolated, the individual daily values may be affected by the sources of error above, leading to underestimates of the actual T_{max}. To attenuate this source of error, we extracted the maximum daily T value within sets of interpolated daily values over 8-day periods, and then selected, for each of the 669 pixels, the highest T observed in any one year as that providing the best estimate of T_{max} for that pixel and year. The dataset can be downloaded from the Pangea open-access data repository (Chaidez et al. 2017)[48].

Calculating decadal trends. The decadal trends of maximum temperatures and time of occurrence were estimated by fitting a linear regression relating T_{max} to year for each of the pixel's yearly time series. The slopes of the fitted linear regressions provide an estimate of the rates of change for each pixel in the Red Sea (units: °C decade^{-1}, and days decade^{-1}, respectively). We tested the possible occurrence of autocorrelation in T_{max} among years, and found, for a sample of pixels, no evidence of autocorrelation, i.e. the T_{max} in any one year is independent of T_{max} in preceding year(s).

Calculating heat anomalies. For each pixel, a reference maximum temperature was computed by taking the mean of the highest temperatures per year over the study period. A heat wave event was defined as a yearly maximum temperature above the reference maximum temperature by a given threshold chosen at 0.5 °C intervals between 0.5 and 1.5 °C. The number of heat wave events over the 34 years were counted for each pixel, as well as the area of the Red Sea experiencing heat waves of various magnitudes in a given year. A Kruskal-Wallis test followed by Dunn's test for multiple comparisons, was used to compare the frequencies of occurrence for all magnitudes of heat anomalies in Fig. 5. The percentage of area in Fig. 6 was calculated as the percentage of pixels. We are aware that the area of each pixel depends on latitude, as the length of a degree longitude varies with latitude. However, for the narrow range of latitude covered by the Red Sea, the difference is minimal, so percent of pixels and area are essentially equivalent.

All data manipulation and analyses were conducted using R (v3.3.1, www.R-project.org)[45].

Data Availability. The data set supporting the analysis presented here can be found in the Pangaea open data repository: (Chaidez *et al.* 2017, http://www.pangaea.de)[48].

References

1. Rhein, M. *et al.* Observations: ocean. In: Climate Change 2013: the physical science basis. Contribution of Working Group I to the Fifth Assessment Report of the Intergovernmental Panel on Climate Change. *Cambridge University Press, Cambridge, United Kingdom and New York, NY, USA* (2013).
2. Poloczanska, E. S. *et al.* Global imprint of climate change on marine life. *Nature Climate Change* **3**, 919–925 (2013).
3. Duarte, C. M., Lenton, T. M., Wadhams, P. & Wassmann, P. Abrupt climate change in the Arctic. *Nature Climate Change* **2**, 60–62 (2012).
4. Marbà, N. & Duarte, C. M. Mediterranean warming triggers seagrass (*Posidonia oceanica*) shoot mortality. *Global Change Biology* **16**, 2366–2375 (2010).
5. Jordà, G., Marbà, N. & Duarte, C. M. Mediterranean seagrass vulnerable to regional climate warming. *Nature Climate Change* **2**, 821–824 (2012).
6. Marbà, N., Jorda, G., Agusti, S., Girard, C. & Duarte, C. M. Footprints of climate change on Mediterranean Sea biota. *Frontiers in Marine Science* **2** (2015).
7. Wilkinson, C. P. The 1997–1998 mass bleaching event around the world. *Status of Coral Reefs of the World: 1998 Report*, *Australian Institute of Marine Science, Townsville, Australia* 23pp. (1998).
8. Lasker, H. R. Gorgonian mortality during a thermal event in the Bahamas. *Bulletin of Marine Science* **76**, 155–162 (2005).
9. Tkachenko, K. S. Impact of repetitive thermal anomalies on survival and development of mass reef-building corals in the Maldives. *Marine Ecology* **36**, 292–304 (2015).
10. Romano, J. C., Bensoussan, N., Younes, W. A. N. & Arlhac, D. Thermal anomaly in the waters of the Gulf of Marseilles during summer 1999. A partial explanation of the mortality of certain fixed invertebrates? *Comptes rendus de l'Academie des sciences. Serie III, Sciences de la vie* **323**, 415–427 (2000).
11. Sparnocchia, S., Schiano, M. E., Picco, P., Bozzano, R. & Cappelletti, A. The anomalous warming of summer 2003 in the surface layer of the Central Ligurian Sea (Western Mediterranean). *Annales Geophysicae* **24**, 443–452 (2006).
12. Coma, R. *et al.* Global warming-enhanced stratification and mass mortality events in the Mediterranean. *Proceedings of the National Academy of Sciences of the United States of America* **106**, 6176–6181 (2009).
13. Lima, F. P. & Wethey, D. S. Three decades of high-resolution coastal sea surface temperatures reveal more than warming. *Nature Communications* **3** (2012).
14. Burrows, M. T. *et al.* The pace of shifting climate in marine and terrestrial ecosystems. *Science* **334**, 652–655 (2011).
15. Burrows, M. T. *et al.* Climate velocity and geographical limits to shifts in species distributions. *Nature* **507**, 492–495 (2014).
16. Fishelson, L. Ecology and distribution of the benthic fauna in the shallow waters of the Red Sea. *Marine Biology* **10**, 113–133 (1971).
17. Belkin, I. M. Rapid warming of large marine ecosystems. *Progress in Oceanography* **81**, 207–213 (2009).
18. Raitsos, D. E. *et al.* Abrupt warming of the Red Sea. *Geophysical Research Letters* **38** (2011).
19. Raitsos, D. E., Pradhan, Y., Brewin, R. J. W., Stenchikov, G. & Hoteit, I. Remote sensing the phytoplankton seasonal succession of the Red Sea. *PloS one* **8** (2013).
20. Kleypas, J. A., Danabasoglu, G. and Lough, J. M. Potential role of the ocean thermostat in determining regional differences in coral reef bleaching events. *Geophysical Research Letters* **35** (2008).
21. Cantin, N. E., Cohen, A. L., Karnauskas, K. B., Tarrant, A. M. & McCorkle, D. C. Ocean warming slows coral growth in the central Red Sea. *Science* **329**, 322–325 (2010).

22. Sherman, K., Belkin, I., Friedland, K. D., O'Reilly, J. & Hyde, K. Accelerated warming and emergent trends in fisheries biomass yields of the world's large marine ecosystems. *AMBIO* **38**, 215–224 (2009).
23. Stillman, J. H. Acclimation capacity underlies susceptibility to climate change. *Science* **301**, 65–65 (2003).
24. Sawall, Y., Al-Sofyani, A., Banguera-Hinestroza, E. & Voolstra, C. R. Spatio-temporal analyses of *Symbiodinium* physiology of the coral *Pocillopora verrucosa* along large-scale nutrient and temperature gradients in the Red Sea. *PloS one* **9** (2014).
25. Roik, A., Roder, C., Rothig, T. & Voolstra, C. R. Spatial and seasonal reef calcification in corals and calcareous crusts in the central Red Sea. *Coral Reefs* **35**, 681–693 (2016).
26. Manasrah, R., Raheed, M. & Badran, M. I. Relationships between water temperature, nutrients and dissolved oxygen in the northern Gulf of Aqaba, Red Sea. *Oceanologia* **48**, 237–253 (2006).
27. Hayes, S. P., McPhaden, M. J. & Wallace, J. M. The influence of sea-surface temperature on surface wind in the eastern equatorial Pacific: Weekly to monthly variability. *Journal of Climate* **2**, 1500–1506 (1989).
28. Chelton, D. B., Schlax, M. G., Freilich, M. H. & Milliff, R. F. Satellite measurements reveal persistent small-scale features in ocean winds. *Science* **303**, 978–983 (2004).
29. Chelton, D. B., Schlax, M. G. & Samelson, R. M. Summertime coupling between sea surface temperature and wind stress in the California Current System. *Journal of Physical Oceanography* **37**, 495–517 (2007).
30. Fishelson, L. Marine reserves along the Sinai Peninsula (northern Red Sea). *Helgoländer Meeresun* **33**, 624–640 (1980).
31. Nykjaer, L. Mediterranean Sea surface warming 1985–2006. *Climate Research* **39**, 11–17 (2009).
32. Thomas, M. K., Kremer, C. T., Klausmeier, C. A. & Litchman, E. A global pattern of thermal adaptation in marine phytoplankton. *Science* **338**, 1085–1088 (2012).
33. Jones, R. J., Hoegh-Guldberg, O., Larkum, A. W. D. & Schreiber, U. Temperature-induced bleaching of corals begins with impairment of the CO_2 fixation mechanism in zooxanthellae. *Plant, Cell and Environment* **21**, 1219–1230 (1998).
34. Maor-Landaw, K. *et al.* Gene expression profiles during short-term heat stress in the red sea coral *Stylophora pistillata*. *Global Change Biology* **20**, 3026–3035 (2014).
35. Hjelle, B. & Glass, G. E. Outbreak of hantavirus infection in the four corners region of the United States in the wake of the 1997-1998 El Niño-Southern Oscillation. *The Journal of Infectious Diseases* **181**, 1569–1573 (2000).
36. Caputi, N., Jackson, G. & Pearce, A. F. The marine heat wave off Western Australia during the summer of 2010/11 – 2 years on. *Fisheries Research Report No. 250. Department of Fisheries, Western Australia* 40pp. (2014).
37. Souvermezoglou, E., Metzl, N. & Poisson, A. Red Sea budgets of salinity, nutrients and carbon calculated in the Strait of Bab-El-Mandab during the summer and winter seasons. *Journal of Marine Research* **47**, 441–456 (1989).
38. Afeworki, Y., Zekeria, Z. A., Videler, J. J. & Bruggemann, J. H. Food intake by the parrotfish *Scarus ferrugineus* varies seasonally and is determined by temperature, size and territoriality. *Marine Ecology Progress Series* **489**, 213–224 (2013).
39. Sawall, Y. *et al.* Extensive phenotypic plasticity of a Red Sea coral over a strong latitudinal temperature gradient suggests limited acclimatization potential to warming. *Scientific Reports* **5** (2015).
40. Ateweberhan, M., Bruggemann, J. H. & Breeman, A. M. Seasonal dynamics of Sargassum ilicifolium (Phaeophyta) on a shallow reef flat in the southern Red Sea (Eritrea). *Marine Ecology Progress Series* **292**, 159–171 (2005).
41. Raitsos, D. E. *et al.* Global climate change amplifies the entry of tropical species into the Eastern Mediterranean Sea. *Limnology and Oceanography* **55**, 1478–1484 (2010).
42. Reynolds, R. *et al.* Daily high-resolution-blended analyses for sea surface temperature. *Journal of Climate* **20**, 5473–5496 (2007).
43. Brasnett, B. The impact of satellite retrievals in a global sea-surface-temperature analysis. *Quarterly Journal of the Royal Meteorological Society* **134**, 1745–1760 (2008).
44. National Climatic Data Center. GHRSST Level 4 AVHRR_OI Global Blended Sea Surface Temperature Analysis. 1st ed. doi:10.5067/GHAAO-4BC01.
45. R Core Team (2013). R: A language and environment for statistical computing. R Foundation for Statistical Computing, Vienna, Austria. www.R-project.org/.
46. H. Wickham (2009) ggplot2: Elegant Graphics for Data Analysis. Springer-Verlag New York.
47. Oscar Perpinan Lamigueiro & Robert Hijmans (2016), meteoForecast. R package version 0.40.
48. Chaidez, V., Dreano, D., Agusti, S., Duarte, C. M. & Hoteit, I. Annual maximum sea surface temperature across the Red Sea (1982–2015). PANGAEA, Dataset #877876 (https://doi.pangaea.de/10.1594/PANGAEA.877876) (2017).

Acknowledgements

This research was funded by King Abdullah University of Science and Technology (KAUST) through the baseline fund to C.M. Duarte, S. Agusti, and I. Hoteit.

Author Contributions

V.C., D.D., C.M.D., S.A., and I.H. conceived and designed the study. V.C. and D.D. acquired the data and created the figures. All authors contributed to the analysis of the results, writing of the manuscript, and approval of the submission.

Additional Information

Competing Interests: The authors declare that they have no competing interests.

Publisher's note: Springer Nature remains neutral with regard to jurisdictional claims in published maps and institutional affiliations.